Fuel 304 (2021) 121371

Contents lists available at ScienceDirect

Fuel

journal homepage: www.elsevier.com/locate/fuel

Full Length Article

Ignition and burning mechanisms of live spruce needles

Adnan Darwish Ahmad [a,*], Ahmad M. Abubaker [a], Ahmad Salaimeh [a], Nelson K. Akafuah [a], Mark Finney [b], Jason M. Forthofer [b], Kozo Saito [a,*]

[a] Institute of Research for Technology Development (IR4TD), University of Kentucky, Lexington, KY 40506, USA
[b] Missoula Fire Sciences Laboratory, US Forest Service, Missoula, MT 59808, USA

ARTICLE INFO

Keywords:
Live fuels
Fire spreading
Forest fire
Scaling analysis
Schlieren
IR imaging

ABSTRACT

Live foliage for some tree and shrub species can support flaming fire spread at much higher moisture content than dead fuel materials. However, the role of live fuels in forest fires has been controversial in the past decades. Although ignition and spread statistical data for live and dead fuels exist in the literature, a clear understanding of the fundamental difference in the burning behavior is missing. To illuminate the role of live fuel on forest fire spreading, a laboratory ignition experiment was designed to examine the burning behavior of live Norway spruce needles. A Schlieren-Infrared combined measurement apparatus was developed with a spatial resolution of 0.75 mm and a time resolution of 0.0025 s, to visualize/measure the ignition behavior of live fuels. Schlieren and IR images revealed that the ejection of live fuel volatiles can alter the flame direction and induce previously unaccounted heating of the nearby fuel. Depending on the conditions, these interferences could heat and modify the heat flux received by the adjacent fuels. To analyze each of these outcomes, a scaling analysis using the law approach was performed. First, theoretical equations were developed and validated against a set of previously published experimental data. After the characteristic equations were verified, we used them to assess the volatile ejection phenomenon. We found that adjacent fuels were preheated by hot volatiles ejected from the heated live needle, and direct flame contact ignited the adjacent fuels. Our IR experiments confirmed the outcomes of the scaling analysis. The rapid ejection of volatiles was also found to propel burning needles far from the burning branch, resulting in micro-spotting.

1. Introduction

Wildland fires have become increasingly destructive, and the associated damage and firefighting costs have increased over the past years. For example, in the U.S. alone, the annual fire suppression budget went from $580 million for the period (1991–2000) to $1.2 billion annually from 2001 to 2010, motivating more fire research [1]. Despite the increased efforts and budget to fight wildland fires, the severity and frequency of wildland fires increased over the past decades [2,3]. An accurate prediction of fire spread rate through wildland fuel beds is important but challenging due to the many different variables involved. Still, firefighters need to predict fire spreading direction and spread rate for their practical firefighting strategy and practice even with the associated uncertainty and fire management personnel to perform strategic planning and decision making [4].

Conifer trees are known to withstand extreme and harsh environmental conditions and are found in a wide range of habitats around the world [5]. Conifer forests extend across continents in the Northern hemisphere [6–9]. This makes the study of conifer fires a worldwide interest, as the ability to protect these natural landscapes is a matter of interest to many countries across the globe. Conifer forests are also susceptible to burning as crown fires, which are characterized by their high intensity and fast rate of spread. Crown fires pose high risks to human populations and natural resources due to a large amount of heat-release and high spreading rates, but the fire spreading mechanism of crown fires is poorly understood [10] due partly to the unknown combustion mechanisms of live crown fuels.

Historically, researchers assumed that live fuels behave as wet dead ones [11]. Studies focused on the moisture content in foliage and its effect on fire spread with that assumption in mind. For instance, Rothermel [12] modeled fire spread in wildland fires, including the effect of fuel moisture content without distinguishing the live and dead fuels. Since then, many researchers have investigated the effect of live fuel moisture content on fire ignition and spread. For instance, in addition to Sun et al. [13], who linked live fuel moisture content (LFMC) with the

* Corresponding authors.
E-mail addresses: Adnandarwish@uky.edu (A. Darwish Ahmad), ksaito@uky.edu (K. Saito).

https://doi.org/10.1016/j.fuel.2021.121371
Received 6 May 2021; Received in revised form 21 June 2021; Accepted 30 June 2021
Available online 10 July 2021
0016-2361/

Nomenclature

c_n	Specific heat capacity of spruce needle, J/(kg.K)
c_s	Specific heat capacity of steam, J/(kg.K)
D_n	Spruce Needle Diameter, m
f	Focal length, mm
h	Heat transfer coefficient, W/(m^{2}K)
k_s	Thermal conduction coefficient, W/(m·K)
l_s	Jet characteristic length
Nu	Nusselt number
Pr	Prandtl number
$Q_{acc,st}$	Heat accumulated in hot boiled volatiles, J
$Q_{acc,needle}$	Heat accumulated inside the needle, J
Q_{cond}	Heat conducted through the needle interior, J
Q_{conv}	Convective heat transfer from jet to the needle, J
Re	Reynolds number
t	Time, s
T	Temperature, K
u_{st}	Volatiles Jetting Velocity, m/s

Greek letters

ρ_n	Density of spruce needle, kg/m^3
ρ_s	Density of steam, kg/m^3
π	Non-dimensional pi number
ν_s	Kinematic viscosity of steam, m^2/s

ignition and spread features of fire, Dennison and Moritz [14] studied the impact of seasonal changes in moisture content over the years and their influences on the fire ignition. More recently, Alexander and Cruz [15] suggested that the normal range of live fuel moisture content (LFMC) has little effect on fire spread rate. Nevertheless, researchers like Rossa and Fernandes [16] examined the monthly values for dead and live fuel moisture content and correlated them with each other, showing why the effect of LFMC on fire rate of spread has been vague, although it does have an influence. Furthermore, Anderson et al. [17] claimed that the correlation between LFMC and the height and bulk density might be the reason for the low effect of LFMC. Although the effect on LFMC was unclear and controversial among researchers, a distinction between live and dead fuels was early demonstrated by Hawley [18] and then followed by Weise et al. [19], where the former's study showed that dead fuel would not sustain flame at moisture contents higher than 35%, and the latter found that fire could spread in live fuels even with doubled or tripled moistures. One reason might be that minor chemical components existing in live spruce needles (terpenes), as seen in [20], have an energy content of approximately 45 MJ/kg, higher than that of gasoline and diesel [21]. However, other studies noted the burning of live fuel leaves with popping and snapping sounds [10]. Even a small burst in the surface of the foliage was noted in some of the experiments conducted by Fletcher et al. [22]; this was tied to the ability of live fuel casing to retain the moisture content inside until its structure is ruptured and the evaporated moisture is violently released [11]. However, the effect of this burning behavior on the fire spread problem has not been studied. The above-mentioned literature suggests that our current understanding of the difference between dead and live fuels is incomplete and Pimont et al. [23] suggests there is an urgent need for understanding the effect of LMFC on fire spread behavior.

There is a rich literature that statistically studied the differences between live and dead fuels in terms of the fire spread rate and ignition. However, a basic understanding of the fundamental differences between the burning behaviors exhibited by the two is still missing [16,19,24]. To answer that question, we developed a hybrid schlieren-IR visualization setup that visualizes the ignition behavior of a freshly cut Norway spruce branch vs. a geometrically similar dead fuel.

The phenomena of "micro-explosions," previously reported as popping sounds, were visualized in live but not dead fuels as expected. These micro-explosions occur as the fire approaches, due to the pressure build-up inside the needle when its moisture evaporates until the needle eventually yields releasing jets of hot volatiles. Characterized by a mixture of water vapor and flammable monoterpenes, those jets can sustain and expand the flame, as visualized by the IR thermography. The following three points summarize the contributions of this paper to the progress in the fire spreading through forest fuel beds.

1. A combined Schlieren-IR visualization of the burning behavior of live vs. dead fuels was performed to explain previously reported live fuel mysteries including the newly observed effect of "micro-explosions" in live fuel.
2. Scaling and IR analyses were conducted based on the above visualization results to theoretically assess the effect of micro-explosions on preheating unburned adjacent spruce needles.
3. A newly observed "micro-spotting" induced by the micro-explosions ejecting ignited needles outside the burning zone comprising new burning zones.

The next section will discuss the details of the experimental methods, sample preparation, accuracy, and reproducibility.

2. Experimental methods

To understand the transient nature of Norway spruce needles heated by flame and characterize the new discreet fire spreading mechanisms, we designed a combined Schlieren and Infrared thermal imaging system, the schematic of which is shown in Fig. 1. Fig. 1(a) depicts the experimental setup schematic while Fig. 1(b) shows the spruce-twig-sample orientation and ignition location, as placed in the test section of the experimental setup. The Schlieren is capable of visualizing jets ejected from the spruce needles and measuring the ejection velocities. The infrared thermography can measure the 2-D temperature profiles of the ejected jets, where both are transient. This is an integrated Schlieren-IR system, which runs simultaneously at about 90°. The idea of this integrated system is traced back to reference [25], where a holographic interferometer and an infrared camera were integrated into one system to successfully measure a transient behavior of spreading flame over liquid fuels. These experimental measurements were then used to construct scaling laws, as explained in later sections. The following details each measurement system.

2.1. Schlieren visualization

The Schlieren experimental setup was previously developed for our study in [26]. The upper part of the schematic in Fig. 1 shows the Schlieren experimental setup to visualize the behavior of the burning Norway spruce needles. The system used an aperture through which 3000 lm of white LED light was passed to approximate a point source. The light faces a 40.6 cm diameter, *f*/4.5 parabolic mirror mounted on an optical table. A knife edge was placed immediately in front of a camera (Phantom Miro 4 camera with a $f = 105$ mm Sigma lens) in the direction towards the test section, for our high-speed Schlieren imaging. A 4,000 *fps* video camera was used to ensure the Schlieren imaging is fast enough to capture the details of micro-explosion and involved transient phenomena.

The Schlieren system's level of illumination in the image plane is proportional to the first spatial derivative of the refractive index of the Schliere gas [27]. Thus, we can capture gas mixtures including hot

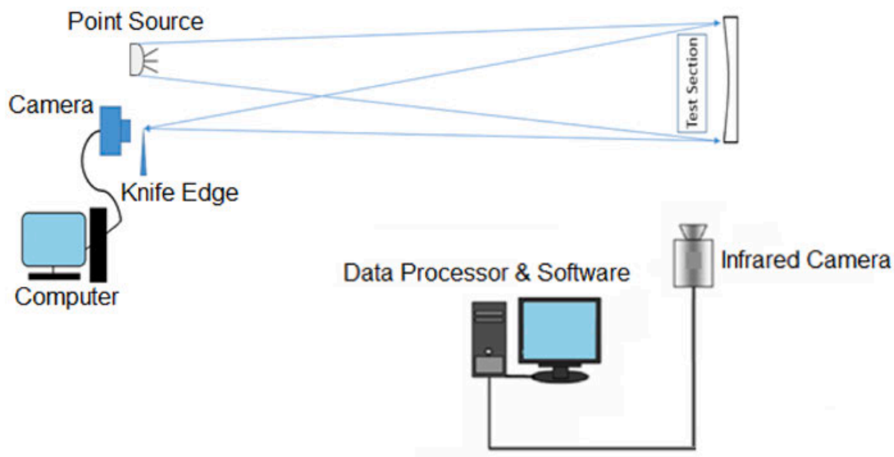

(a)

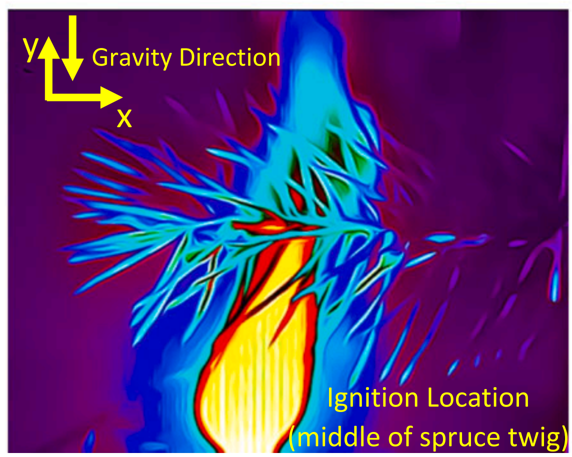

(b)

Fig. 1. (a) Schematic of the integrated Schlieren-Infrared thermography system, (b) Tested sample orientation and ignition location.

convection plumes, combustion gases, and gaseous products of pyrolysis, in the testing section of a different refractive index from the surrounding air where they appear as illuminance contrast (dark streaks/Schlieren) in the image plane. Our Schlieren system is capable of adjusting the visualization contrast by raising the knife-edge [28]. However, this system has trade-offs: the higher the visualization contrast, the more illumination is required.

2.2. Sample preparation

The wildland fuel samples were collected from the area of Lexington, Kentucky, USA (38.0406° N, 84.5037° W). The tests of live needles followed the sample preparation procedure provided in reference [29] to ensure the sample preparation method is compatible with other researchers and the results are reproducible. The freshly cut Norway spruce small branches were immediately taken for experimental testing. Following the procedure in reference [29], the ignition tests were conducted within the first hours of collection to minimize loss of the chemical constituents or moisture content. The ignition experiments were repeated at least 30 times to ensure a reliable database and nearly 100% repeatability because this step is crucial for the following scaling analysis. Using the experimental setup shown in Fig. 1, we placed the freshly cut Norway spruce needle sample at the test section, ignited it by an external flame source, and observed the temporal behavior of the heated spruce needles: ignition to the micro explosion of the needle (ejection of the vapor), as described in the previous section. It is worth mentioning that we conducted a series of preliminary ignition tests using a propane torch flame, a soft-flame lighter, and a small candle flame. Regardless of these different types of pilot flames and heat inputs that we applied; the ignited spruce needles all exhibited micro-explosions. Smaller pilot flames, however, gave us clearer Schlieren and IR images of the micro-explosions compared to larger pilot flames. This because on the image plane, the larger combustion plumes associated with the larger pilot flames covered the micro-explosions, and the latter could not be distinguished clearly. Therefore, in this study, we present the ignition experiments from the regular soft-flame lighter, due to its slower ignition process that allowed us to clearly observe the effect of micro-explosions on the flame dynamics and the adjacent needles.

2.3. Infrared thermography temperature measurement

We have developed a unique Infrared thermography technique [30] that is able to accurately measure the location of active pyrolysis during upwardly spreading fires along a vertically suspended wall surface [31]. We have also developed a uniformly heated blackbody background technique to visualize the dynamical behavior of small droplets ejected from a high-pressure nozzle [32,33]. With these systems and methods available, the temperature of the spruce vapor jets ejected from the heated needles was measured.

Fig. 2a shows a schematic of the IR calibration system against the heated blackbody, which emits radiation to the infrared camera. The blackbody emitter used was an IR-160/301™ Blackbody System; it extended an area of (304.8 × 304.8 mm^2), consisting of a flat plate emitter with a high emissivity coating (average emissivity = 0.96), and with temperature-controlled within ± 0.1 °C resolution. A ThermoVision™ SC4000 infrared camera was used for two-dimensional thermal imaging, calculating intensities and temperatures for each imaged pixel [34], and measuring spectral wavelengths of 3–5 μm [35]. The IR video used a 400 *fps* imaging and an integration time of 0.05 *ms*, over which the IR intensity measurements were calibrated using the blackbody to read temperatures.

During the experiments, the temperature of the blackbody was set to 35 °C and the IR intensity count was recorded with the IR camera. Then, the blackbody temperature was increased to 40 °C, and counts were recorded again. The same procedure was repeated up to 215 °C in a 5 °C increment. After completing this incremental increase in temperature calibration, the temperature was decreased back again to 35 °C in a 5 °C decrements, and the intensity counts were measured by the infrared camera in the increasing and decreasing temperature phases, averaging the intensity count values to be used as the temperature calibration, as shown in Fig. 2b.

3. Results and discussion

3.1. Visualization results

In contrast with dead fuel burning behavior, burning with popping sounds, propulsion of ignited live fuel conifer needles, and flame deflections and expansions in all directions was a repeated characteristic systematically exhibited by the burning live conifer branches and consistently observed over the course of our experiments. It is well known that the live fuels can retain the moisture content within their cellulosic cell structure, which is abruptly released as moisture evaporates and the needle is ruptured, for instance, during burning, making those popping sounds, while dead fuels, on the other hand, release water content through diffusion [11]. When the approaching fire heats spruce needles, liquid trapped inside the needle evaporates, building pressure inside the needle case until it finally ruptures, and the hot vapor is violently ejected. The terms micro-explosion and steam/volatiles ejection will be used interchangeably in this study.

To visually investigate this burning behavior of live conifer fuels, Fig. 3(a-d) show a time series of four Schlieren images (the top row) and the bottom row shows the corresponding four schematic diagrams (a-d). Fig. 3(a) time = 0 shows the onset of micro-explosion which took place at the end of a spruce twig heated by a flame shown in the schematic as well. Fig. 3(b) time = 0.025 s after the onset of micro-explosion shows the jet ejection area to expand further. Fig. 3(c) time = 0.05 s shows a continuous expansion of the jet ejection area indicating an increased rate of volatile release by mico-explosion. Finally, Fig. 3(d) shows the end of a mico-explosion event. Note that the nature of events shown in Fig. 3(a-d) was not sporadic but highly repeatable with the same time order of magnitude shown in Fig. 3.

Fig. 4(a) shows a Schlieren image of igniting a single dead needle with Fig. 4(a) (bottom) showing the corresponding schematic along with a dimensional scale. The dead needle showed a steady burning with a constant flame spreading rate. Contrary to the dry needle, Fig. 4(b) (top part) shows a Schlieren image of igniting a single live spruce needle with Fig. 4(b) (bottom) showing the corresponding schematic. The burning characteristic difference between the dead and the live needles as shown in Fig. 4 is strikingly different.

A careful analysis of the high-speed Schlieren video images which we used to create Fig. 4 revealed that the dead needle burns completely as the flame spreads from one end of the sample to the other. The live needle once heated, would violently release the cell content as seen in Fig. 4(b). Furthermore, to test the prevalence of this phenomenon, we repeated the live needle ignition experiment on 20 randomly selected needles, and found out that 20 of them exhibited the same behavior seen in Fig. 4(b), meaning that this micro-explosion behavior is not random, and prevails among burning live spruce needles. Now the question to be asked is: what role these micro-explosions play in spreading fire?

The IR imagery revealed the impact of these explosive events altering the trajectory of the flame and heat transfer within a heated spruce twig. Fig. 5(a) shows the burning twig immediately before the micro-explosion occurs, and Fig. 5(b) shows the flame deflected by the micro-explosion event. As seen from the figure, the flame is initially in the upright position (normal position driven by bouyancy) igniting the middle section of the spruce twig. However, as the micro-explosion occurs, it expands the flame in the lateral direction, inducing heat transfer in directions that are not typical in its absence. In addition to the flame deflection, Fig. 5(b) revealed that the ejected volatile vapors can support and promote flaming. To clarify and explain these observations, a schematic is created and shown in Fig. 5(c). As mentioned in the experimental section, these experiments were repeated more than 30 times under the same laboratory conditions over a year and recorded in IR videos. A careful review of these IR videos confirmed the Fig. 5 events to be repeatable and not seasonally dependent.

Another outcome was also observed when the jet ejections do not interfere with the flame but directly impinge on the adjacent fuels. This can be seen in the IR images shown in Fig. 6 (top part) and the corresponding schematic (bottom). Micro-explosions could have two consequences for heat transfer and fire spread. First, the jets can expand the flame in the direction of the adjacent needles causing intermittent heating by flame bathing. Second, the hot volatiles impinge directly on an adjacent needle without interfering with the flame and directly preheat the adjacent needles by the convective flow of the hot jets.

This outcome is dependent on the size of the flame itself. For

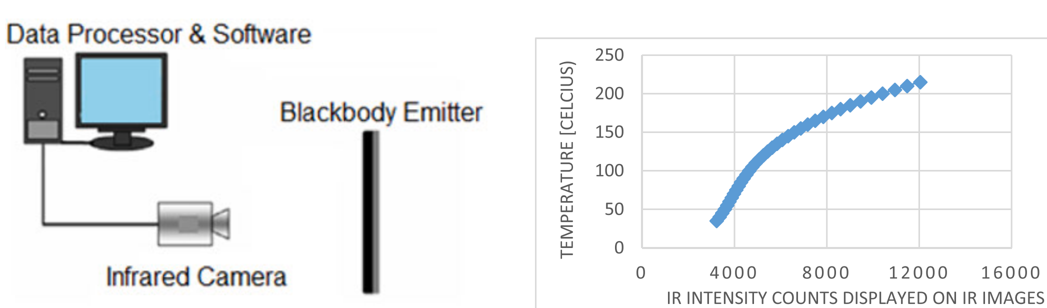

(a) Schematic of the Infrared set up (b) Resulting Calibration Curve

Fig. 2. Infrared calibration.

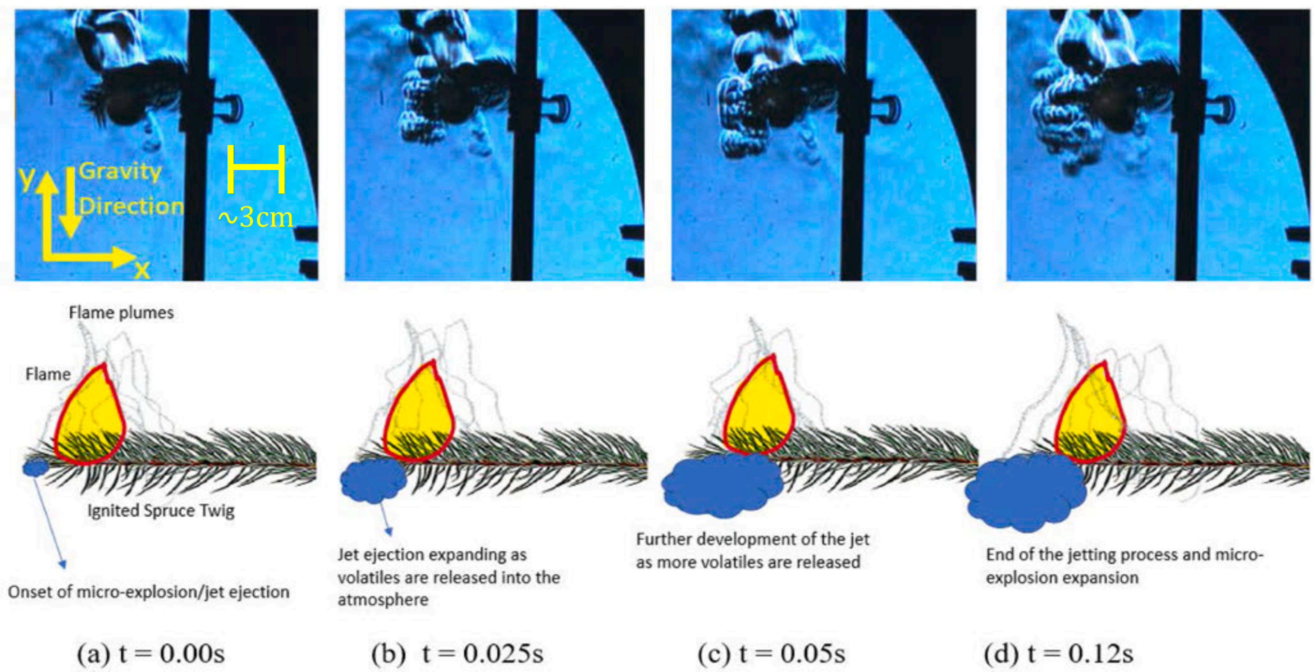

Fig. 3. Series of four Schlieren images (top row) showing the process of micro-explosion in burning live Norway spruce needles and the corresponding schematics (bottom row).

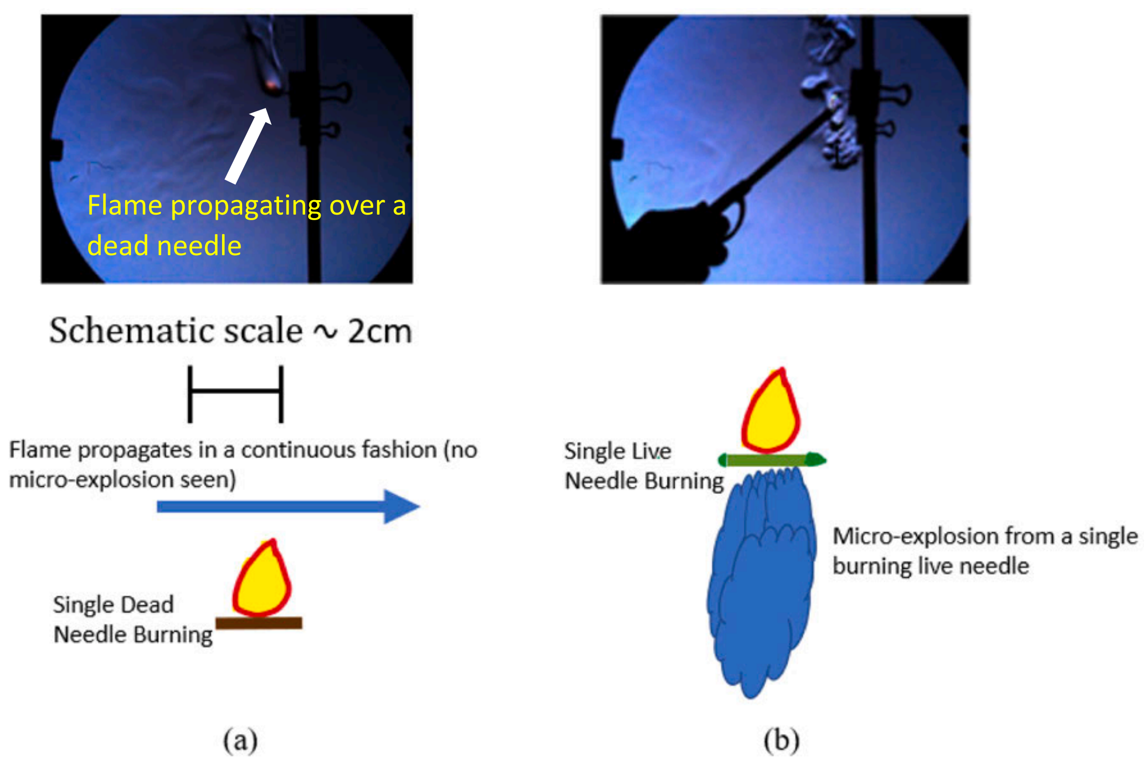

Fig. 4. (a) A Schlieren photograph showing dead needle burning (top) and the corresponding schematic and schematic scale (bottom) and (b) A Schlieren photograph showing micro-explosion (top) for a heated live spruce needle and the corresponding schematic (bottom).

instance, when smaller flames are used, it is more probable that the jets can pass without interfering with the fire, i.e., will not ignite but rather directly impinge on the adjacent needles. However, as the size of the flame grows larger, the jets are more likely to pass close to the flame and ignite, causing flame impingement rather than direct jet impingements. This effect is discussed in detail later in this article.

It is worth noting that not all volatile ejections support flaming since the ejected jets comprise a mixture of water vapor with the highly flammable volatile resins and monoterpenes found in live fuels. The ratio of the flammable chemical component of volatiles to the moisture content for a particular live fuel, which was not investigated in this study, is expected to influence the behavior of fires, therefore remains

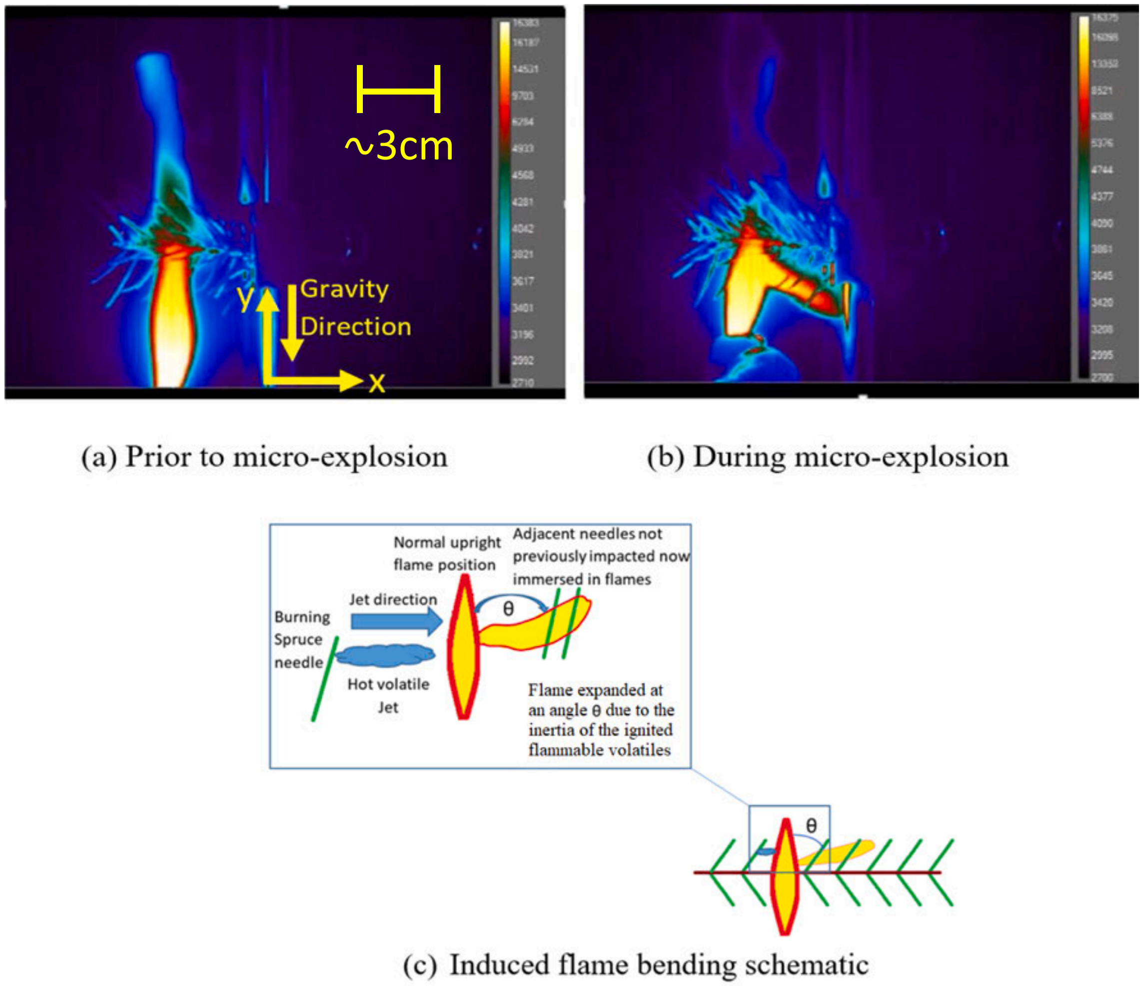

Fig. 5. IR thermal images to show micro-explosion-induced flame bending and schematics to explain the flame bending phenomenon.

for future study. Also, it should be mentioned that the flame expansions investigated in this study are a result of the rapid ignition of the flammable volatiles and tiny atomized droplets ejected during the jets release. The point of examination of the current work is the effect these volatiles/tiny droplets have after they ignite and impinge on the adjacent needles. As such, a relevant question is whether these micro-explosion events exist long enough to heat or ignite the adjacent fuel materials. The next section is dedicated to answering this question.

3.2. Scaling analysis with the law approach

Three different approaches are available in formulating the dominant non-dimensional groups (Pi numbers) that governs a phenomenon, namely, the equation approach, the parameter approach, and the law approach [36,37]. Since the governing equations of any phenomena are dimensionally homogenous, it follows that they can be rearranged in non-dimensional groups. This means the Pi numbers can be formulated by this rearrangement and manipulation process, and this is what we call the equation approach. Although this approach is a powerful tool for obtaining all dimensionless numbers related to a phenomenon, unfortunately, it returns all Pi numbers, but without any insight into which are dominant, and instead produces equally weighted dimensionless numbers [38]. In the parameter approach, also known as the Buckingham Pi theorem, a group of parameters assumed to be related to the phenomenon must be chosen, and then they are non-dimensionalized one by one using the parameters in the selected group until only non-dimensional numbers remain. The problem associated with the parameter approach is the selection of parameters; unfortunately, the choice of a physical parameter often will not result in a successful nondimensionalization process. Since the initial parameter choice can lead to a failed process, nondimensionalization can become an iterative process. This leads us to the last approach initially developed by Emori [39] and further developed by Saito [36]; the law approach. Since the main rationale of scaling depends on the dynamic similarity between the actual size model and the prototype, in this last method, the phenomenon must be observed carefully to decipher the potential governing forces or energy terms dominating the problem. Then those governing terms are written in terms of characteristic rather than the specific parameters, from which different ratios are built generating the dominant Pi numbers. This method is simple yet very effective in formulating the scaling laws as can be seen in studies on fires and fire-related events [1,31,36,37,39–43].

To examine the effect of flame bathing and direct jet impingements on the preheating of the adjacent fuels, we first identified the major energies and formulated the corresponding equations using characteristic parameters and pi-numbers, then validated them against published experimental data on the piloted live fuel ignition [24]. After the comparison with experimental data yielded very good accuracy, we applied the validated equations to form key pi-numbers that control preheating and ignition by micro-explosion. Finally, we conducted further IR experiments to validate the conclusions drawn from the scaling analysis. We chose here to apply the law approach [37,39] to derive scaling laws by identifying the major heats that govern the current problem as this approach is simple, yet very effective as aforementioned. The first step of

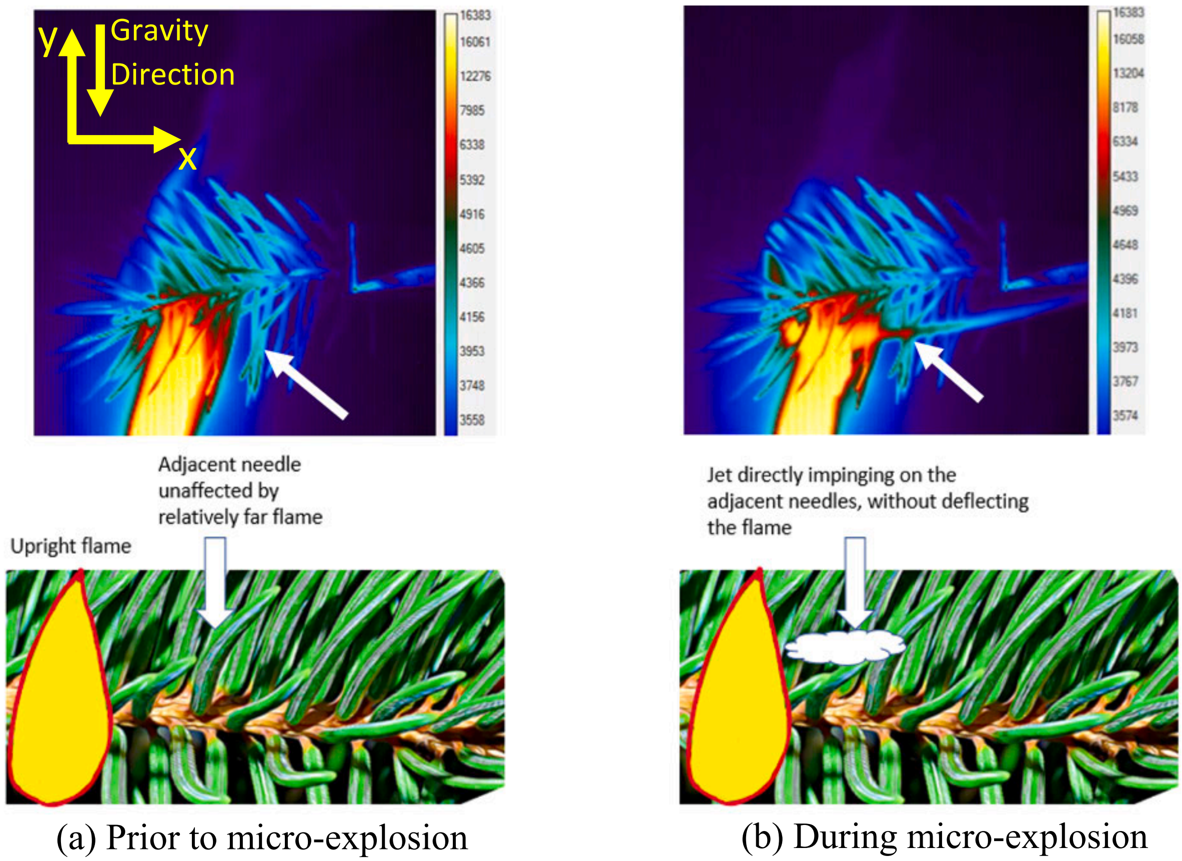

Fig. 6. Two IR thermal images of direct jet impingements on adjacent needles (top left: before micro-explosion, and top right: during micro-explosion) and the corresponding color images explaining these observed events (bottom).

the law approach [37] begins with the assumption to identify major heats involved in preheating of adjacent needles by the micro explosion. To assist that process, Fig. 7 shows a schematic created based on the Schlieren and IR thermal images showing the heat transfer process from a hot micro-explosion jet flowing over a cold spruce needle and dumping the heat to it. The spruce needle is represented by a millimeter-diameter cylinder and the convective flow is two-D laminar.

The following five major heats are assumed to govern this micro-explosion heating process. The heat accumulated in the gas phase jets, $Q_{acc,st}$, corresponding to the heat-source term, the convective heat transfer from the jet to the adjacent cold needle surface, Q_{conv}, that is the heat transferred into the surface of the needles from the jets by

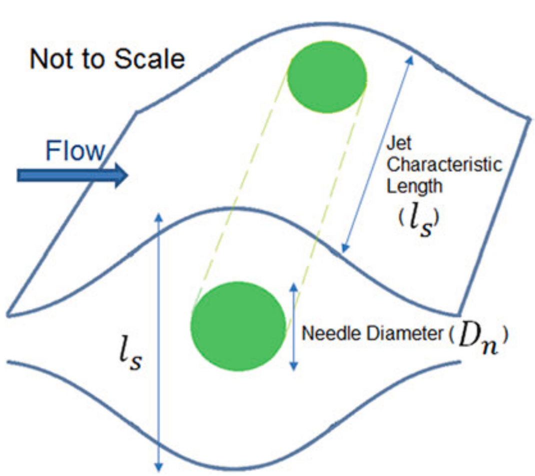

Fig. 7. Configuration of jet flowing over a needle.

convective currents, the heat conducted from the surface of the needle to the interior, Q_{cond}, the sensible heat accumulated inside the needle, $Q_{acc,needle,sensible}$, and the latent heat of vaporization of the moisture content, Q_{λ}.

We describe each of these heats using characteristic parameters in Eqs. (1) through (5) as aforementioned. The energy accumulated in the gaseous phase is proportional to the mass of that phase, its specific heat capacity, and the temperature difference between the hot gases and the ambient. Therefore, from observations of the schlieren videos, the mass was estimated by how much gaseous phase (jets) flow through during the puffing time, where the jets were assumed to be cylindrically flowing over adjacent needles, and the characteristic parameters were obtained from the schlieren and IR videos. The convective term is estimated through the contact area between the jets and the spruce needles as seen in Fig. 7, multiplied by the coefficient of convective heat transfer, temperature difference, and the convective time needed for the heat to be transferred to the surface of the needles. The conduction term is derived by substituting characteristic parameters in the Fourier conduction equation and multiplying the heat rate obtained by the conduction time. To assess the conduction heat passing from the surface of the needle to the center, the diameter of the needle is used as the characteristic length. Finally, the sensible accumulation term inside the needles, similar to the first term, is proportional to the mass of the needle embedded inside the hot jet as seen in Fig. 7, and to the specific heat capacity and the temperature difference between ambient and that required for ignition to take place. The latent heat accumulation term is tied to the energy required for phase change (boiling moisture content inside the needle).

$$Q_{acc,st} = \rho_{st} \times \frac{\pi}{4} \times l_{st}^{2} \times u_{st} \times t_{puff} \times c_{st} \times \Delta T \quad (1)$$

$$Q_{conv} = h \times \pi \times D_n \times l_s \times \Delta T \times t_{conv} \quad (2)$$

$$Q_{cond} = k_n \times D_n \times \Delta T \times t_{cond} \quad (3)$$

$$Q_{acc,needle,sensible} = \rho_n \times \frac{\pi}{4} \times D_n^2 \times l_s \times (1 - MC\%) \times c_n \times \left(T_{ig} - T_{amb}\right) + \rho_n \times \frac{\pi}{4} \times D_n^2 \times l_s \times MC\% \times c_{st} \times \left(T_{boiling} - T_{amb}\right) \quad (4)$$

$$Q_{\lambda} = \rho_n \times \frac{\pi}{4} \times D_n^2 \times l_s \times MC\% \times h_{fg} \quad (5)$$

Since moisture content varies for different live fuels, the ratio between $Q_{acc,needles,sensible}$ and Q_{λ} will also vary accordingly, therefore, to ensure the generality of the resulting estimations using the formulated equation, $Q_{acc,liveneedle}$, which is the total energy (including both sensible and latent heats) was used for the total heat accumulation term inside the live needles. This is the total energy that must accumulate in the needle's mass consisting of both dry and liquid for any moisture content value for ignition to take place. The specific formulation for $Q_{acc,liveneedle}$ is shown in Eq. (6).

$$Q_{acc,liveneedle} = \rho_n \times \frac{\pi}{4} \times D_n^2 \times l_s \times (1 - MC\%) \times c_n \times \left(T_{ig} - T_{amb}\right) + \rho_n \times \frac{\pi}{4} \times D_n^2 \times l_s \times MC\% \times \left(h_{fg} + c_{st} \times \left(T_{boiling} - T_{amb}\right)\right) \quad (6)$$

As such, the four governing heats associated with the micro- explosion heating process becomes: $Q_{acc,st}$, Q_{conv},Q_{cond},$and Q_{acc,liveneedle}$. Since these equations will be used to test the effect of the jets on preheating and ignition of the adjacent live fuels, it would help to use them to predict ignition-time behaviors and compare them with existing reliable live fuel ignition data for accuracy assessment.

McAllister et al [24] conducted heating and ignition experiments of live and dead needles to investigate their ignition-time behavior difference. They used a radiant source for heating a square sample of a single layer of needles in a wind tunnel, varying the heat flux at each time and measuring the ignition time for various types of dead and live fuels. The governing heat equations to theoretically assess the ignition times in [24] consist of four heat terms, Q_{flux}, Q_{conv}, Q_{cond}, $Q_{acc,liveneedle}$, which are essentially the same energy terms in our Eqs. (1)–(3) and Eq. (6). Note that their heating source term corresponds to the micro-explosion heating in our equation allowing us to predict the heating time to ignition using the law approach. The heating configuration that McAllister used in their experiments was not the same as the one shown in Fig. 7. Therefore, the estimation of the terms in the equations above had to be modified accordingly to theoretically predict the ignition results from their experiment. For instance, as aforementioned, the heat source term in their experiment was a radiant source. Consequently, the heat energy provided is proportional to the product of the flux investigated and the sample area multiplied by the time it takes to ignite the sample, where the latter is the unknown to be estimated. Additionally, the convective cooling term in [24], had to be subtracted from the energy supplied by the radiant source. The convective term was, as shown in Eq. (2), proportional to the heat convection coefficient multiplied by the area and the convection time. The sample used in [24] was a square plate, hence, the convective coefficient must be estimated accordingly, and the time duration of convection loss was that it takes for ignition to occur, i.e. ignition time. Finally, for ignition to take place the heat must accumulate inside the needles, and therefore must be conducted first. As such, the heat conducted inside the sample is equal to the heat accumulation shown in Eq. (6). Using an order of magnitude estimates of the thermophysical properties and an average value of moisture content obtained from [10], then equating the accumulation term to the radiant heat energy minus the convective losses, leaves one unknown in the equation; the ignition time. Table 1 shows thermophysical properties used for our calculations and Fig. 8 compares the measured

Table 1
Thermophysical properties of steam and Norway spruce needles.

Steam Properties @ ~ 177 °C [48]			Needle properties		
Physical Quantity	Value	Units	Physical Quantity	Value	Units
ρ_s	0.49	$[\frac{kg}{m^3}]$	D_n	10^{-3}	$[m]$
k_s	$29.9*10^{-3}$	$[\frac{W}{m.K}]$	α_n	$1.94*10^{-7}$	$[\frac{m^2}{s}]$
ν_s	$31.11*10^{-6}$	$[m^2/s]$	k_n	0.135	$[\frac{W}{m.K}]$
l_s	$3*10^{-3}$	$[m]$			
c_s	$1.98*10^3$	$[\frac{J}{kg.K}]$			
Average Velocity magnitude order	~1	[m/s]			
Initial Ejection Velocity magnitude order	~10	[m/s]			

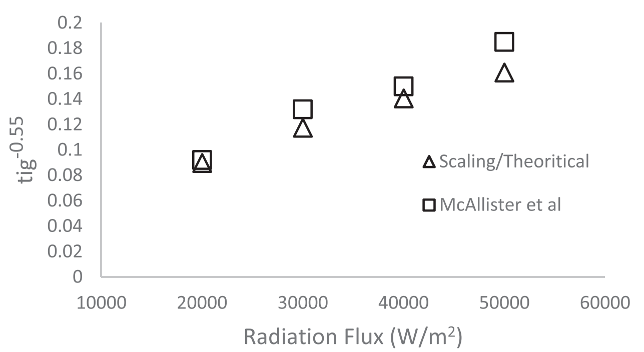

Fig. 8. Comparison of ignition time data [24] with the ignition time predicted from our scaling analysis.

experimental ignition time for live fuels with our theoretical estimations obtained by the scaling analysis and the characteristic parameters. Excellent agreement in Fig. 8 between experimental measurements and scaling estimations made it possible to confidently conduct the following scaling analysis using the equations formulated by the law approach. Without detailed knowledge of the composition of cell contents and constituents of the jets during burning, we assumed them to have the same properties as steam for a first-order approximation. Therefore the steam properties were used to approximate those of the mixture, whose prediction was favorable compared with experimental data in Fig. 8. This agreement supports our assumption for the use of water vapor to represent the physical properties of fuel volatiles for the micro-explosion scaling.

Now that we know the scaling analysis can provide a good estimate of the ignition behavior, we proceed to further explore the effect of the micro-explosions on the heating process of the adjacent "cold" fuels. Table 1 was used again for the thermophysical properties of the jets and needles to estimate the heat transfer characteristic since these parameters yielded a good comparison with experimental data. The choice of the temperature at which the steam properties were evaluated, was tied to the temperature approximations from the IR thermal images of the jets. The temperature of the jets was estimated to be ~130–180 °C based on the results from the calibration experiment. These values were in good agreement with boiling temperatures of Alpha-Pinene and delta-3-carene which forms most of the monoterpene emissions in Norway spruce and Scot pines [20], respectively having a boiling temperature of 156 °C [44] and (175–178) °C [45]. It is worth noting that the exact constituent of those jets is not currently known, therefore, the emissivity cannot be accurately estimated. However, the actual emissivity of these jets could only be lower than that of the blackbody used for the calibration. Therefore, the reported temperatures are a conservative lower limit indicating that the jets will more effectively preheat the adjacent needles to their higher temperatures. Additionally, as the IR-measured spectral intensities are approximately related to the temperature raised to the power of four, this means that the temperatures will not change drastically with moderate emissivity changes. Additionally, according to [46], the emissivity of the many plant's leaves is close to that of a blackbody. This means that the needles' temperatures as visualized in the IR videos is accurate. The thermophysical properties for conifer-type needles were published in the work by Kerr et al. [47] and are also shown in Table 1.

Additionally, the velocity of the jets was needed for the scaling calculation. To that end, we took a painstaking process to carefully review the Schlieren and IR videos and obtained images that were perpendicular to our camera. We also took simultaneous Schlieren and IR videos at 90°and the jet speed was determined from the ejection perpendicular to the Schlieren camera. Fig. 9 shows four time-series Schlieren images and the corresponding schematic. Analyzing the first frames in the videos, the initial ejection velocity of 10 m/s was obtained. This value agrees with the velocity of erupted jet calculated by Zhang et al [49] but is one order of magnitude higher than the average velocity (~1 m/s) calculated based on the distance traveled by the jet from ejection to stop, divided by the time taken. The average velocity is used in Eq. (1) to estimate the energy in the volatile jets. Substituting the values in table one in Eqs. (1)–(6) and noting that the puffing time measured from the IR videos was found to be 0.1–0.4 s, the following order of magnitude estimate was obtained among the four governing heats: $Q_{acc,st} \sim Q_{conv} \sim 0.1$J, $Q_{acc,liveneedle} \sim Q_{cond}$ is a corollary for ignition as was explained in the validation part, where $Q_{acc,liveneedle} \sim 1$J. This outcome results in Eq. (7). It is worth mentionning that the orders of magnitude considered here are only associated with the part of the needle embedded in the jet, as was shown in Fig. 7.

$$Q_{acc,liveneedle} > Q_{acc,st} \tag{7}$$

This means that hot jets have enough energy to heat the surface of the adjacent needles, but cannot result in ignition. That is because their temperature is not high enough and their residence time is not long enough to cause ignition. On the other hand, if the temperature of the jets is close to that of the flame, i.e. the heating occurs through flame impingements rather than direct jet impingements, then Eq. (7) would change to Eq. (8), since the jets accumulation and convection terms' order of magnitude would change to $Q_{acc,st} \sim Q_{conv} \sim 1$J in that case; i.e., the flame impingements having enough energy to heat the adjacent needles to ignition temperature.

$$Q_{acc,liveneedle} \sim Q_{acc,st} \tag{8}$$

As such, direct impinging of jets onto the adjacent needles will only preheat the fuel, but not ignite them. If the micro-explosions blow through the flame and expand it towards the adjacent needles which are then heated by direct flame contact, then ignition is possible. This analysis showed that the key non-dimensional number to evaluate the effect of micro-explosions on the heating process is; $\pi_{jets} = \frac{Q_{acc,st}}{Q_{acc,liveneedle}}$. When $\pi_{jets} \geq 1$, the micro-explosions are likely to result in ignition from the intermittent impingements.

This π_{jets} formulation shows a close resemblance of the Semenov theory of ignition [50], which predicts ignition by equating the net heat flux received by the fuel (equal to heat generation minus heat losses) to the accumulation term inside the fuel. In our micro-explosion case, we represent this net heat flux into the fuel by the Q_{conv} which in this case is of the order of $Q_{acc,st}$ as shown in Eq. (7), and the accumulation in the fuel needed for ignition by $Q_{acc,liveneedle}$. To obtain the parametric equations for the π_{jets} in terms of the characteristic parameters in their simplest form, the formulation will be broken down into two cases; namely, direct jet impingement and flame impingement. Some assumptions and order of magnitude estimation are needed for each scenario. Let the ΔT in Eq. (1) be ΔT_1, $(T_{ig} - T_{amb})$be ΔT_2 and $(T_{boil} - T_{amb})$ be ΔT_3. For most fuels, T_{ig} is of the order of 350 °C making $\Delta T_2 \sim 325$ °C. An average boiling of volatile monoterpenes was considered, so $T_{boil} \sim 150$ °C making $\Delta T_3 \sim 125$ °C. These two approximations hold for both, direct jet and flame impingements. As for ΔT_1 the case is different, since this temperature difference depends on the heating source temperature. For the case of jet impingements, ΔT_1 is the difference between the jets and ambient temperatures, i.e. ΔT_1 is equal to $\Delta T_3 \sim 125$ °C. For the flame impingements case, $\Delta T_1 \sim 900$ °C. Using these assumptions, the two simplified form of the π_{jets} become as follows:

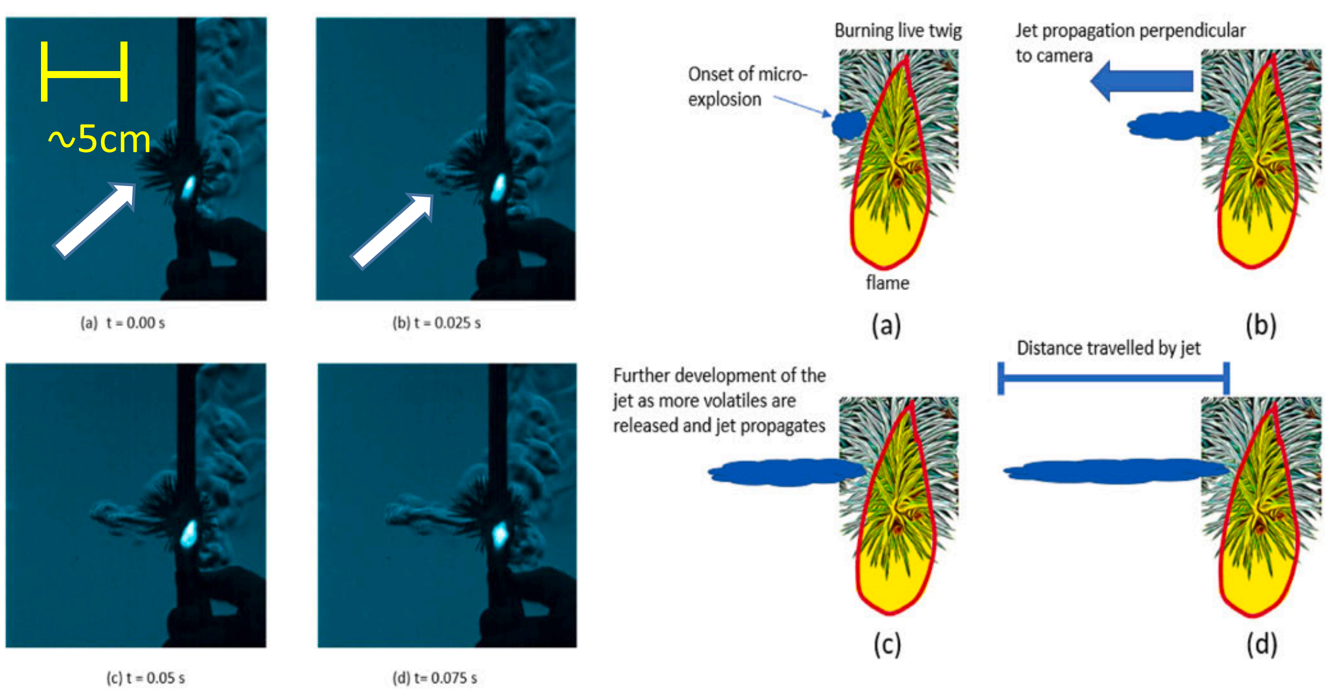

Fig. 9. Temporal development of a micro-explosion.

$$\pi_{jets,direct} = \frac{\rho_{st} \times l_{st} \times u_{st} \times t_{puff} \times c_{st} \times \Delta T_1}{\rho_n \times D_n^2 \times [3(1 - MC\%) \times c_n \times \Delta T_1 + MC\% \times (h_{fg} + c_{st} \times \Delta T_1)]} \tag{9}$$

and

$$\pi_{jets,flame} = \frac{\rho_{st} \times l_{st} \times u_{st} \times t_{puff} \times c_{st} \times \Delta T_1}{\rho_n \times D_n^2 \times \left[\frac{1}{3}(1 - MC\%) \times c_n \times \Delta T_1 + MC\% \times \left(h_{fg} + \frac{c_{st} \times \Delta T_1}{7}\right)\right]} \tag{10}$$

Further simplification can be achieved by noting that $h_{fg} > c_{st}\Delta T_1$, so omitting the terms $c_{st}\Delta T_1$ and $\frac{c_{st}\Delta T_1}{7}$ from Eqs. (9) and (10) respectively can yield a more simple version of the equations with roughly 80% prediction accuracy. Note that in extreme cases, for instance, if a fuel of T_{ig} much higher or much lower was being investigated, or in cases where volatile compounds have much higher or lower boiling temperatures, and the assumptions used to derive the simplified π_{jets} in Eqs. (9) and (10) no longer hold, the original definition of the π_{jets} alongside Eqs. (1) and (6) could still be used by substituting the extreme values for the particular case in hand.

To test this outcome of the scaling analysis, further IR investigations of the post; jet and flame impingements were observed to validate the expectations of the scaling. Fig. 10a shows IR image of post-jet impingement and Fig. 10b shows post-flame impingement, confirming our scaling analysis results, i.e., mico-explosion jets preheat unburned fuels, while flame bathing ignites the fuel. On the contrary, previous researchers focused on the concurrent wind effect on wildland fires [51,52] created by an increase in the flame angle with the vertical to heat unburned fuels by radiation and convection, thus, leading to an increased rate of fire spread. They attempted to understand the effect of the natural wind on the fire spread rate but not the micro-explosion-induced wind. The intermittent buoyancy-induced flame impingement effects were also studied by Finney et al. [53]. However, none of the previous studies investigated the intermittent heating by the micro-explosion exhibited by live fuels.

We showed here that the jet ejection from live spruce needles can produce local "latent wind", even when the natural wind is absent. This latent wind momentum (caused by micro-explosion) deflects the flame towards the adjacent needles, as shown in the IR image of Fig. 5(b) and schematic in 5(c), has the similar (but at a smaller scale) effect mentioned by these authors [51,52], i.e., bending the flame intermittently towards the unburnt fuel and hence preheating the adjacent fuels by increasing flame azimuth angle, also by intermittent impingement of fire as discussed by Finney et al. [53]. However, as aforementioned, the latter discussed intermittent heating by flame impingement due to buoyancy-induced effects, while in this work, the intermittent heating was a result of live fuel micro-explosion-induced effects.

Raman et al. [21] showed that alpha-pinene, one of the characteristic volatile monoterpenes found in pine trees, had more energy density than most biofuels and even higher than gasoline. This finding supports one of the hypotheses explaining how live fuels can sustain flaming combustion. Our current study also showed that flammable volatiles can enhance the heat transfer rate by the induced intermittent impingements. Raman's demonstration and our current study explain the main reasons why live fuels are able to sustain fires even at higher moisture contents compared to dead fuels as was mentioned by Finney et al. and Weise et al. [11,19].

It is worth mentioning that these micro-explosions continue to take place while live fuels are burning ejecting jets in all 3-D directions, causing the flame bathing of adjacent twigs and branches. In conifer trees, the branches are stacked, and these intermittent impingements will cause the adjacent fuels to be heated and therefore more readily spread the moving fire, which in turn is also flame bathing the adjacent fuels due to the buoyancy effects as explained by Finney et al. in [53]. Fig. 11a shows the flame in a normal upright position transferring heat to unburnt fuel by radiation and convection as already known without micro-explosions. Then the flame is tilted by the volatile jets to impinge on adjacent branches creating the scenario shown in Fig. 11b, where the second flame was tilted by micro-explosion increasing radiation and convection heat transfer received by the adjacent needles. This flame spreading pattern will continue until all conifer needles on the same branch are consumed. Fig. 11c depicts how a 3D micro-explosion looks like on a conifer tree, preheating adjacent fuels by jet impingements, a precondition enhancing the fire spread.

Concluding all preceding results and discussion, as explained by Finney et al. in [53,54], fine particles and needles which make most of the wildland fuels, cool effectively by free and forced convection remaining below ignition temperatures until flame impingements occur. These studies pointed out the importance of flame dynamics and the role of convection in the ignition process. Adam et al. [55] proposed a St^{-1} $-Fr^{-1}$ relation governing various scales of fire, as small as a candle flame to as large as a typical wildfire, which was later confirmed by Finney et al. in [53]. This scaling relationship bolstered the role of buoyant flames and vortex shedding in the intermittent heating of the unburnt fuels through flame impingements, and their importance pertaining to ignition.

The same argument holds, where the micro-explosions resemble an

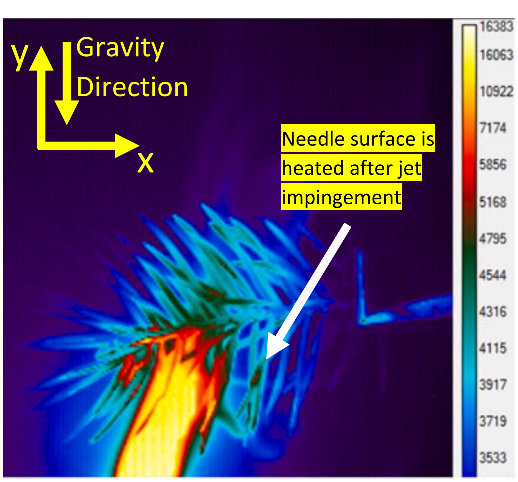

(a) Post jet impingement

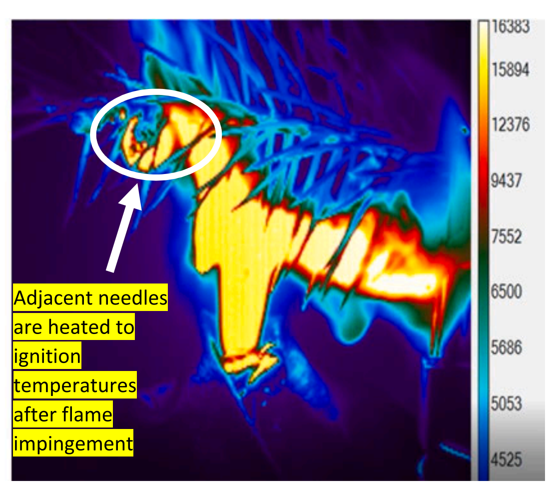

(b) Post flame-impingement

Fig. 10. Adjacent spruce heated by jet and flame impingement.

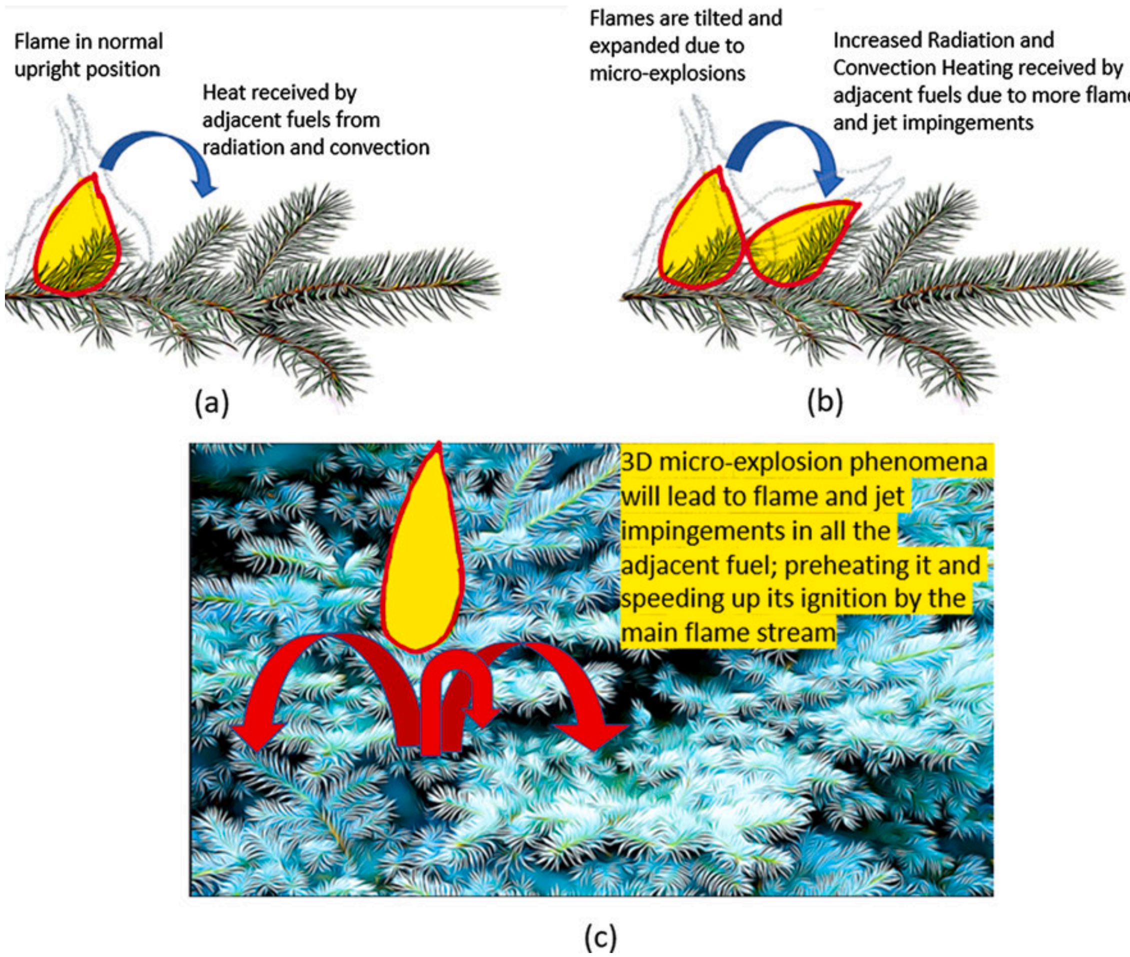

Fig. 11. Schematic describing the micro-explosion effect on fire spreading: (a) upright flame heating adjacent spruce needles by radiation and convection (b) the flame impingements on the adjacent branch caused by micro-explosion which tilts the flame and preheats the adjacent needles, and (c) a 3D micro-explosion preheating branches in all directions in a conifer tree.

important contributor to the intermittent flame impingements as was demonstrated in this article; meaning that live fuels' content must be accounted for in the flame dynamics and heating mechanisms as well.

Following the same line of thought in [55], Fig. 12 resembles a proposed $\pi_{jets} - l_{fire}$ (where $l_{fire}$is the flame characteristic length), showing how the π_{jets} is anticipated at different fire scales, and its effect on the heating process of the adjacent fuels. Note that the l_{fire} characterizes the size of the flame and is not the same as the size of the micro-explosion denoted by l_{st}. At a small-scale fire, down to a single needle burning, depicted by small flame characteristic lengths (small l_{fire}), the micro-explosions are more likely to impinge directly on adjacent needles as aforementioned, i.e., π_{jets} can be estimated as $\pi_{jets,direct}$ from equation (9). As flame size grows larger, and fire is more embedded within the fuels, such as on a branch scale, jets are more likely to interfere with the flame and ignite, flame bathing the adjacent unburnt fuels, therefore, π_{jets} can be estimated as $\pi_{jets,flame}$ from equation (10). This means that π_{jets} becomes of the order of magnitude of one and jet impingements can result in ignition, which is supported by the observation of live fuels being able to support flaming ignition better on a branch level.

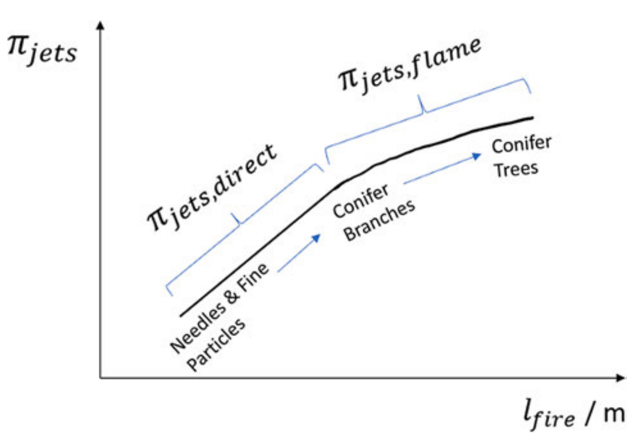

Fig. 12. Proposed π_{jets} dependence on characteristic flame length in wildfires.

As fire grows larger, radiation can preheat nearby fuels and although radiation heat by itself is not sufficient to cause ignition [54], it can help lower the fuel's moisture content; reducing the accumulation term in Eq. (6). Since the accumulation term in the gaseous phase remains unaffected, the $\pi_{jets,flame}$ value should increase as seen in Fig. 12, supporting the flaming process. It is expected that this number can only increase to a certain maximum with the increasing size of the flame, where the drying adjacent fuels reach a critical moisture content and ignite before further change in the accumulation term in Eq. (6). Although this proposed graph can be explained by the scaling laws of burning needles and branches, tests on larger scales, including conifer tree fires and wildland fires must be conducted to verify the proposition. Validation of such graph requires a huge set of quantitative data at various fire scales; needles, branches, trees, and wildlands. Therefore, it is crucial is to investigate the effect of different sized flames/burning rates on the dominancy of the micro-explosions as a heating mechanism where the proposed non-dimensional graph is constructed based on quantitative data, similar to what was done in the two research works of Adam and Finney [53,55]. This will confirm the scale at which the micro-explosions play a vital role in the fire spread problem as a heating mechanism and determines how they interact with different size flames. The latter investigation is crucial to understand how the flame bathing via micro-explosions compares to the radiation and convection heat transfer mechanisms at various flame sizes, particularly larger flames, which will tell us when these live fuel heating mechanisms must be considered and when they can be neglected.

Furthermore, it is worth mentioning that jet flames have the ability to withstand higher wind blow-off limits compared to soft flames. For instance, torch lighters can withstand higher winds as compared to soft-flame lighters. This analogy to torch against soft lighters can be corelated to live vs dead fuels burning behaviors respectively, as was seen in Fig. 4. As such, live fuels which exhibits jetting flame behaviors, would be able to support the flame during higher winds, particularly on large fire scales when the π_{jets} is high due to higher flame contact probability. This generates a dangerous condition for fire spread and can explain the extremely high rate of spread seen in live fuel fires on high-wind days, such as the Campfire that occurred in Paradise, California in 2018.

3.3. Micro-spotting in live fuels

Spotting fires have always been thought of as an event resulting from the large fire convection plumes lifting firebrands and moved by buoyancy/wind current to start fires in the area outside the fire perimeter as studied by Albini [56–58]. Fig. 13 shows a time series of five Schlieren photographs of burning Norway spruce needles: (a) is the onset of micro-spotting, t = 0.00 s, (b) t = 0.05 s, (c) t = 0.10 s, (d) t = 0.15 s, and (e) t = 0.20 s. As to fire-heated spruce needles, when the heated needle

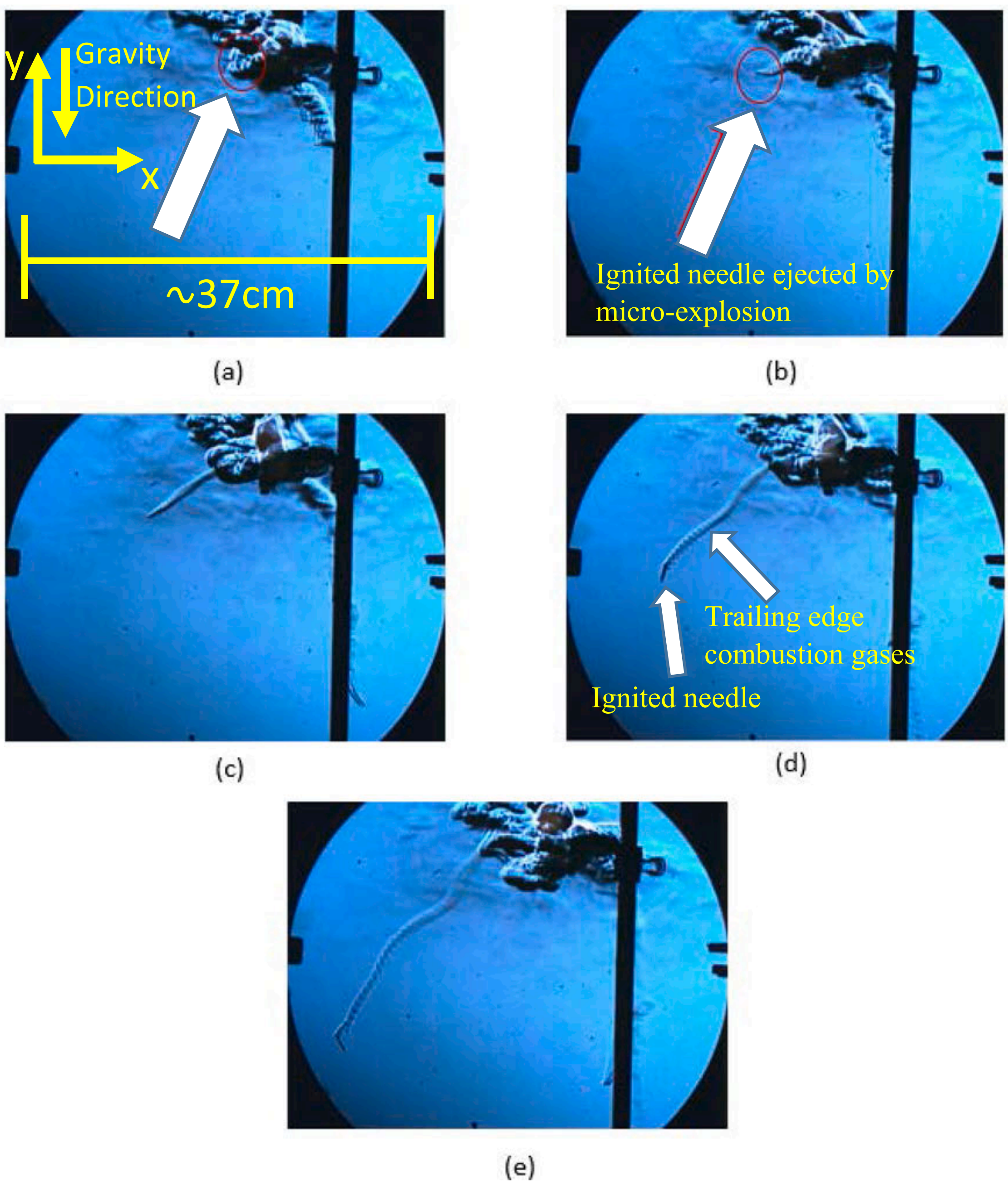

Fig. 13. A series of five Schlieren photographs of burning Norway spruce needles: (a) the onset of micro-spotting at t = 0.00 s, followed by (b) t = 0.05 s, (c) t = 0.10 s, (d) t = 0.15 s, and (e) t = 0.20 s.

ruptured, the needle's boiled volatiles ejected can throw hot needles to further distances, as can be seen in Schlieren photographs (c)–(e).

This indicates that live Norway spruce needles heated by the approaching fire can transfer fire outside of the immediate burning zone of the flame by this micro-spotting phenomenon. This micro-spotting concept may be analogous to large-scale spotting fires by firebrands in forest fires [59].

Acting forces on the firebrands in large-scale forest fires are the inertial force of wind and the buoyancy force provided by the fire [59], while for the micro-spotting, the pressure-driven momentum force of the ejected jets due to the micro explosion plays the major role. The governing forces for these two phenomena are different, but both exhibit a discreet fire spreading mechanism [60]. For that reason, we call these two phenomena analogous based on the definition of the analogous model [36].

Fig. 14 shows two IR images of ignited needles ejected outside the burning zone. These ignited needles can start a fire in nearby branches analogous to large-scale forest spotting fires, and that the maximum micro-spotting distance along with the probability of ignition would be a good potential future study to examine the effect of this fire eruption behavior.

4. Conclusions

(1) Live fuels contain complex constituents that actively engage in the fire dynamics of burning Norway spruce needles. The micro-explosion-induced ejection of boiled fuel vapors from spruce needles was found to enhance heat transfer to adjacent unburned spruce needles by forced convection and direct flame bathing. Our scaling analysis showed a high possibility that the hot jets ejected from the burning needle can raise the temperature of the adjacent needles' surface, preheating them closer to their ignition temperature.

(2) Scaling analysis using the law approach, showed that during a direct jet impingement, the $Q_{conv} < Q_{acc,liveneedle}$, meaning that the jets can only preheat the nearby needles, but cannot raise their temperatures to ignition. However, when the flammable jets interfere with the flame and expand it towards the adjacent needles, the equation becomes, $Q_{conv} \sim Q_{acc,liveneedle}$, meaning that those flame impingements have enough energy to raise the temperature of the adjacent fuels to ignition temperatures.

(3) The jets can also change the flame angle resulting in increased radiation due to higher azimuth angles which support flaming.

(4) Small scale spotting of ignited parcels was evident as a result of the live fuel "micro-explosion" inertia which ejected burning needles outside the burning zones.

(5) This study revealed that the heat transfer mechanism that can sustain fire spreading in live conifer needles is a discrete mode (not continuous) consisting of micro-explosion in live needles and the resulted micro spotting.

This paper suggests similar investigations to examine different species and the effect of various moisture contents on the heating, spotting, and flame expanding behaviors is an important consideration. Specific

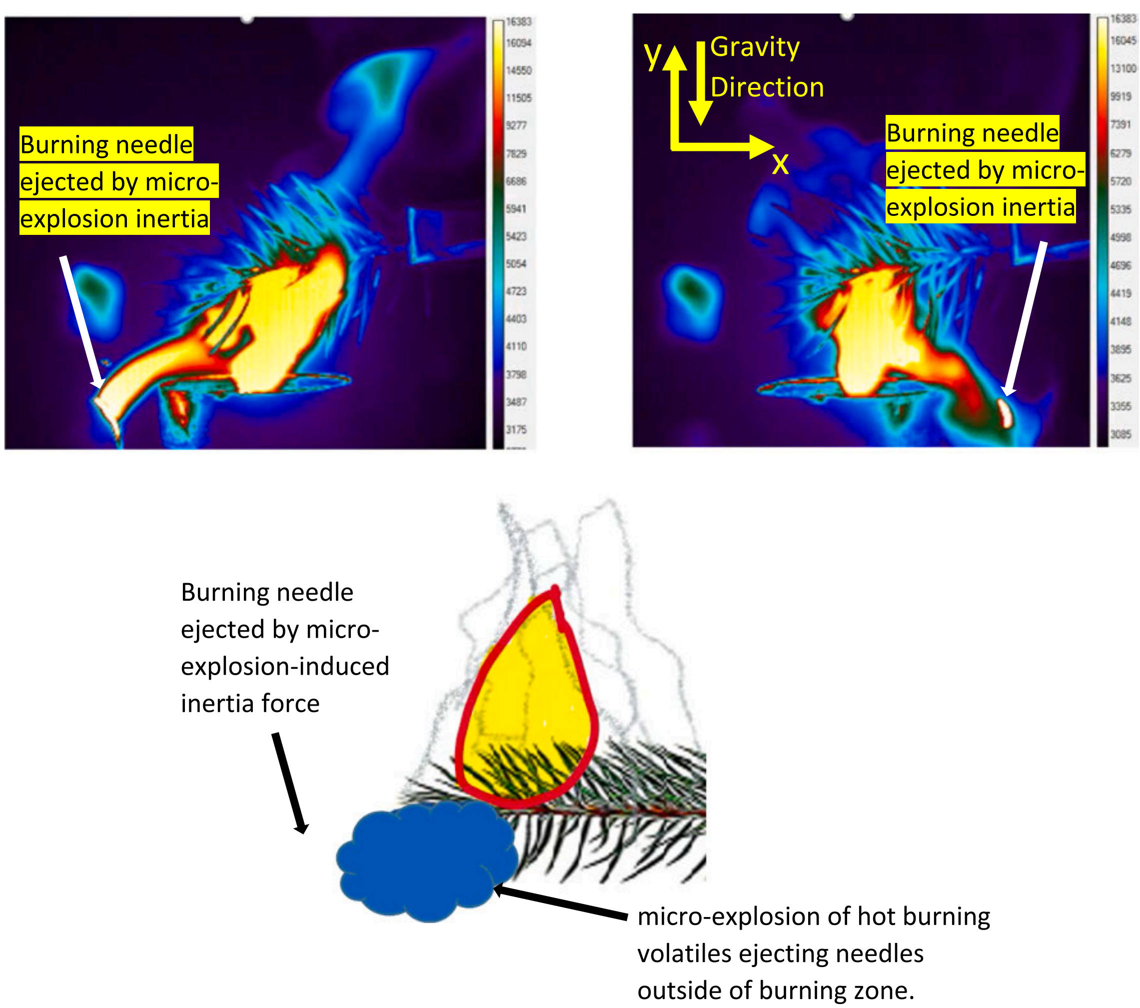

Fig. 14. Ignited needles ejected by micro-explosions outside burning parameter.

effects of micro-explosions on the maximum spotting distance and the probability of ignition are important future considerations, as well as the cumulative effect of this latent wind in actual forest fires where dense trees entrain larger spaces.

CRediT authorship contribution statement

Adnan Darwish Ahmad: Conceptualization, Methodology, Formal analysis, Visualization, Investigation, Data curation, Writing - original draft, Validation, Writing - review & editing. **Ahmad M. Abubaker:** Writing - original draft, Visualization, Investigation, . **Ahmad Salaimeh:** Conceptualization, Supervision. **Nelson K. Akafuah:** Conceptualization, Writing - original draft, Supervision. **Mark Finney:** Conceptualization, Writing - original draft, Supervision. **Jason M. Forthofer:** Conceptualization, Writing - original draft. **Kozo Saito:** Conceptualization, Methodology, Formal analysis, Data curation, Writing - original draft, Writing - review & editing, Supervision.

Declaration of Competing Interest

The authors declare that they have no known competing financial interests or personal relationships that could have appeared to influence the work reported in this paper.

Acknowledgments

This study was funded by USDA Forest Service under grant number 17-CS-11221637-099. We thank Binit Singh for his assistance in the infrared calibration experiments, and Tianxiang Li for his invaluable comments and editing.

References

[1] Gustenyov N, Akafuah NK, Salaimeh A, Finney M, McAllister S, Saito K. Scaling nonreactive cross flow over a heated plate to simulate forest fires. Combust Flame 2018;197:340–54.
[2] Stephens SL, Ruth LW. Federal forest-fire policy in the United States. Ecol Appl 2005;15(2):532–42.
[3] Dennison PE, Brewer SC, Arnold JD, Moritz MA. Large wildfire trends in the western United States, 1984–2011. Geophys Res Lett 2014;41(8):2928–33.
[4] Thompson M, Calkin D, Scott JH, Hand M. Uncertainty and probability in wildfire management decision support. Natural Hazard Uncertainty Assessment: Modeling and Decision Support; 2017. p. 31–41.
[5] Rodrigues-Corrêa KCDS, Lima JC, Fett-Neto AG. Pine oleoresin: tapping green chemicals, biofuels, food protection, and carbon sequestration from multipurpose trees. 1. 2012:81-93.
[6] Peichl M, Moore TR, Arain MA, Dalva M, Brodkey D, McLaren J. Concentrations and fluxes of dissolved organic carbon in an age-sequence of white pine forests in Southern Ontario, Canada. Biogeochemistry 2007;86(1):1–17.
[7] Seniczak S, Dabrowski J, Klimek A, Kaczmarek S. Effects of air pollution produced by a nitrogen fertilizer factory on the mites (Acari) associated with young Scots pine forests in Poland. Appl Soil Ecol 1998;9(1-3):453–8.
[8] Izhaki I, Henig-Sever N, Ne'Eman G. Soil seed banks in Mediterranean Aleppo pine forests: the effect of heat, cover and ash on seedling emergence. J Ecol 2000;88(4): 667–75.
[9] Mabuhay JA, Nakagoshi N, Horikoshi T. Microbial biomass and abundance after forest fire in pine forests in Japan. Ecol Res 2003;18(4):431–41.
[10] McAllister S, Weise DR. Effects of season on ignition of live wildland fuels using the forced ignition and flame spread test apparatus. Combust Sci Technol 2017;189(2): 231–47.
[11] Finney MA, Cohen JD, McAllister SS, Jolly WM. On the need for a theory of wildland fire spread. Int J Wildland Fire 2013;22(1):25–36.
[12] Rothermel RC. A mathematical model for predicting fire spread in wildland fuels. Res Pap INT-115 Ogden, UT: US Department of Agriculture, Intermountain Forest and Range Experiment Station 40 p 1972;115.
[13] Sun L, Zhou X, Mahalingam S, Weise DR. Comparison of burning characteristics of live and dead chaparral fuels. Combust Flame 2006;144(1-2):349–59.
[14] Dennison PE, Moritz MA. Critical live fuel moisture in chaparral ecosystems: a threshold for fire activity and its relationship to antecedent precipitation. Int J Wildland Fire 2010;18(8):1021–7.
[15] Alexander ME, Cruz MG. Corrigendum to: Assessing the effect of foliar moisture on the spread rate of crown fires. Int J Wildland Fire 2013;22(6):869–70.
[16] Rossa CG, Fernandes PM. On the effect of live fuel moisture content on fire-spread rate. Forest Syst 2018;26(3):08.
[17] Anderson WR, Cruz MG, Fernandes PM, McCaw L, Vega JA, Bradstock RA, et al. A generic, empirical-based model for predicting rate of fire spread in shrublands. Int J Wildland Fire 2015;24(4):443. https://doi.org/10.1071/WF14130.
[18] Hawley L. Theoretical considerations regarding factors which influence forest fires. J Forest 1926;24(7):756–63.
[19] Weise DR, Zhou X, Sun L, Mahalingam S. Fire spread in chaparral—'go or no-go?'. Int J Wildland Fire 2005;14(1):99–106.
[20] Janson RW. Monoterpene emissions from Scots pine and Norwegian spruce. J Geophys Res: Atmos 1993;98(D2):2839–50.
[21] Raman V, Sivasankaralingam V, Dibble R, Sarathy SM. α-Pinene-A High Energy Density Biofuel for SI engine applications. SAE Technical Paper 2016.
[22] Fletcher TH, Pickett BM, Smith SG, Spittle GS, Woodhouse MM, Haake E, et al. Effects of moisture on ignition behavior of moist California chaparral and Utah leaves. Combust Sci Technol 2007;179(6):1183–203.
[23] Pimont F, Ruffault J, Martin-StPaul N, Dupuy J-L. Why is the effect of live fuel moisture content on fire rate of spread underestimated in field experiments in shrublands? Int J Wildland Fire 2019.
[24] McAllister S, Grenfell I, Hadlow A, Jolly WM, Finney M, Cohen J. Piloted ignition of live forest fuels. Fire Saf J 2012;51:133–42.
[25] Konishi T, Ito A, Kudo Y, Narumi A, Saito K, Baker J, et al. Simultaneous measurement of temperature and chemical species concentrations with a holographic interferometer and infrared absorption. Appl Opt 2006;45(22): 5725–32.
[26] Darwish Ahmad A, Abubaker A, Salaimeh A, Akafuah N. Schlieren Visualization of shaping air during operation of an electrostatic rotary bell sprayer: impact of shaping air on droplet atomization and transport. Coatings 2018;8(8):279.
[27] Settles GS. Schlieren and shadowgraph techniques: visualizing phenomena in transparent media. Springer Science & Business Media; 2012.
[28] Mazumdar A. Principles and techniques of Schlieren imaging systems. Columbia University Computer Science Technical Reports 2013:14.
[29] Reszka P, Cruz JJ, Valdivia J, González F, Rivera J, Carvajal C, et al. Ignition delay times of live and dead pinus radiata needles. Fire Saf J 2020;112:102948.
[30] Arakawa A, Saito K, Gruver W. Automated infrared imaging temperature measurement with application to upward flame spread studies. Part I. Combustion and flame 1993;92(3):222-IN2.
[31] Saito K, Quintiere J, Williams F. Upward turbulent flame spread. Fire safety science-proceedings of the first international symposium. 1986:75-86.
[32] Akafuah NK, Salazar AJ, Saito K. Estimation of liquid volume fraction and droplet number density in automotive paint spray using infrared thermography-based visualization technique. Atom Sprays 2009;19(9):847–61.
[33] Darwish Ahmad A, Singh BB, Doerre M, Abubaker AM, Arabghahestani M, Salaimeh AA, Akafuah NKJF. Spatial positioning and operating parameters of a rotary bell sprayer: 3D mapping of droplet size distributions. 2019;4(3):165.
[34] Akafuah NK, Salazar AJ, Saito K. Infrared thermography-based visualization of droplet transport in liquid sprays. Infrared Phys Technol 2010;53(3):218–26.
[35] Akafuah NK. Visualization and characterization of ultrasonic cavitating atomizer and other automotive paint sprayers using infrared thermography. (Doctoral dissertation), Department of Mechanical Engineering, University of Kentucky 2009.
[36] Emori R, Saito K, Sekimoto K. Scale models in engineering (Mokei Jikken no Riron to Ohyou). Gihodo Publishing Co, Tokyo, Japan 2000;20(0):0.
[37] Saito K, Williams F. Scale modeling in the age of high-speed computation. Progress in Scale Modeling, Volume II. Springer; 2015, p. 1-18.
[38] Williams F. Scaling mass fires. Fire research abstracts and reviews. 11. Washington, DC: The National Academies Press; 1969.
[39] Emori RI, Schuring DJ. Scale models in engineering: Fundamentals and applications. Elsevier; 2016.
[40] Emori I, Iguchi Y, Saito K, Wichman I. Simplified scale modeling of turbulent flame spread with implication to wildland fires. Fire Saf Sci 1989;2:263–73.
[41] EMORI RI, SAITO K. A study of scaling laws in pool and crib fires. Combust Sci Technol 1983;31(5-6):217–31.
[42] Kuwana K, Sekimoto K, Saito K, Williams FAJFSJ. Scaling fire whirls. 2008;43(4): 252-7.
[43] Soma S, Saito K. Reconstruction of fire whirls using scale models. Combust Flame 1991;86(3):269–84.
[44] National Center for Biotechnology Information. PubChem Compound Database; CID=6654, https://pubchem.ncbi.nlm.nih.gov/compound/6654 (accessed Oct. 29, 2018).
[45] National Center for Biotechnology Information. PubChem Compound Database; CID=26049, https://pubchem.ncbi.nlm.nih.gov/compound/26049 (accessed Nov. 8, 2018).
[46] López A, Molina-Aiz FD, Valera DL, Peña A. Determining the emissivity of the leaves of nine horticultural crops by means of infrared thermography. Sci Hortic 2012;137:49–58.
[47] Kerr J, Buck C, Cline W, Martin S, Nelson W. Nuclear weapons effects in a forest environment. thermal and fire. General Electric Co Santa Barbara CA DNA Information and Analysis Center; 1971.
[48] Incropera FP, Lavine AS, Bergman TL, DeWitt DP. Fundamentals of heat and mass transfer. Wiley; 2007.
[49] Zhang W, Zussman E, Yarin AL. Heat and mass transfer resulting in eruptive jetting from stems and leaves during distillation stage of forest fire. Exp Therm Fluid Sci 2020;116:110112.
[50] Williams FA. Combustion Theory Benjamin. Menlo Park: Cummings; 1985.
[51] Lozano JS. An investigation of surface and crown fire dynamics in shrub fuels. UC Riverside; 2011.

[52] Viegas DX. On the existence of a steady state regime for slope and wind driven fires. Int J Wildland Fire 2004;13(1):101–17.
[53] Finney MA, Cohen JD, Forthofer JM, McAllister SS, Gollner MJ, Gorham DJ, et al. Role of buoyant flame dynamics in wildfire spread. Proc Natl Acad Sci 2015;112 (32):9833–8.
[54] Finney MA, Forthofer J, Grenfell IC, Adam BA, Akafuah NK, Saito K. Section B fire and explosion-A study of flame spread in engineered cardboard fuel beds Part I: Correlations and observations of flame spread. Progress in scale modeling, Volume II. Springer; 2015. p. 71–83.
[55] Adam BA, Akafuah NK, Finney MA, Forthofer J, Saito K. Section B Fire and Explosion-A Study of Flame Spread in Engineered Cardboard Fuel Beds Part II: Scaling Law Approach. Progress in Scale Modeling, Volume II. Springer; 2015, p. 85-95.
[56] Albini FA. Potential spotting distance from wind-driven surface fires. US Department of Agriculture, Forest Service, Intermountain Forest and Range Experiment Station; 1983.
[57] Albini FA. Spot fire distance from isolated sources: extensions of a predictive model. US Dept. of Agriculture, Forest Service, Intermountain Forest and Range Experiment Station; 1981.
[58] Albini FA. Spot fire distance from burning trees. 1979.
[59] Manzello SL, Suzuki S, Gollner MJ, Fernandez-Pello ACJPiE, Science C. Role of firebrand combustion in large outdoor fire spread. 2020;76:100801.
[60] Williams FA. Urban and wildland fire phenomenology. Prog Energy Combust Sci 1982;8(4):317–54.